

The AISI 317L and SAF 2304 Steels Pitting Corrosion Resistance in Acidified Glycerin from Biodiesel Production

F. L. Menezes^{a,b*} , M. M. R. Castro^b, V. F. C. Lins^b 

^aInstituto Federal do Norte de Minas Gerais, 39404-058, Montes Claros, MG, Brasil.

^bUniversidade Federal de Minas Gerais, 31270-901, Belo Horizonte, MG, Brasil.

Received: September 11, 2023; Revised: December 24, 2023; Accepted: February 20, 2024

Austenitic and lean duplex stainless steels, such as AISI 317L and SAF 2304, present high mechanical and corrosion resistance, which make them alternative materials for biodiesel plant equipment. Because there is not sufficient research about these stainless steel-specific applications, this work aims to evaluate AISI 317L and SAF 2304 stainless-steel pitting corrosion resistance in a chloride-containing acidified glycerin solution, collected directly from a biodiesel plant. The SAF 2304 presented a higher pitting potential than the AISI 317L, at room temperature and at service temperature, 337 K. However, the SAF 2304 passive layer was more reactive than the AISI 317L, showing a higher passive current density in the polarization and chronoamperometric tests. Furthermore, the Mott–Schottky technique showed that the passive layer of the AISI 317L steel contained a lower concentration of defects than the passive layer of the SAF 2304, and the oxides of the passive layers are n-type semiconductors.

Keywords: *Pitting corrosion, glycerin, chloride, AISI 317L, SAF 2304, polarization.*

1. Introduction

The wide use of fossil fuels brings climatic and economic consequences, such as environmental pollution, atmospheric warming, and the dispute over petroleum reserves caused by its inevitable depletion^{1,2}. Several research about the use of biodiesel as a clean and renewable energy have been developed to reduce petroleum consumption³⁻⁵. Biodiesel is obtained from a transesterification reaction. It is a reaction between vegetable oils, animal fats or waste grease, and a short chain alcohol, in the presence of a catalyst. The biodiesel production generates glycerin as a byproduct^{6,7}.

Strong bases, such as sodium or potassium hydroxide, are used as the reaction catalyst in biodiesel industries. For the neutralization of the alkaline catalyst, a diluted hydrochloric acid is used⁸. However, the use of a hydrochloric acid solution promotes localized corrosion on the production process equipment⁸⁻¹⁰. Pitting corrosion is one of the most common and dangerous forms of localized corrosion in passive metals and commonly occurs in aggressive environments such as bromide and chloride solutions^{9,11}.

Some authors have studied stainless-steel corrosion using biodiesel as the medium¹²⁻¹⁴, but literature about stainless-steel corrosion from chloride-containing acidified glycerin, collected directly from biodiesel processes, is scarce¹⁵⁻¹⁹.

Austenitic stainless steels (ASS) usually exhibit good corrosion resistance, due the passivation layer formed on their surface, which is composed of iron and chromium oxides²⁰⁻²⁵. The localized corrosion resistance is increased by the molybdenum addition to the ASS. Furthermore, molybdenum promotes the passivation layer stabilization^{25,26}.

Duplex stainless steels (DSS) are also resistant to corrosive environments. They show good mechanical

properties due to the ferrite (α) phase existence and have a high corrosion resistance because of the austenite (γ) phase presence. Those phases are present in almost equal volume fraction. However, they can be embrittled, have their good corrosion properties affected, and the working temperature limited to 350 °C by a secondary phase precipitation, such as σ (sigma) or χ (chi) and other particles or phases such as Cr_2N (chromium nitrides) or α' (alpha prime)^{27,28}. Duplex stainless-steel passivation layer is stabilized by chromium and the nickel chemical content^{29,30}. In lean duplex steels, nickel and molybdenum content is reduced compared with duplex stainless steels with the aim to reduce cost, which is compensated by increasing manganese and nitrogen content to ensure the austenite phase formation^{11,29}.

Literature has proved that SAF 2304 lean duplex stainless-steel corrosion resistance is comparable to the AISI 316L austenitic stainless steel^{29,31}. From earlier studies, the AISI 317L presents higher corrosion resistance than the AISI 316L stainless steel. Likewise, it can be expected that AISI 317L austenitic stainless steel has better corrosion resistance than SAF 2304 lean duplex steel. In this way, this research aims to find a steel that has better corrosion resistance than the steel 304L in a chloride-containing acidified glycerin solution from a biodiesel plant, at 337K, service temperature. It is known that AISI 317L and SAF 2304 have higher corrosion resistance than 304L, but there is no research that compares both stainless steels in this specific solution and temperature. It makes this work interesting and useful for further research and industrial processes.

In this paper, the localized corrosion resistance of the AISI 317L austenitic stainless steel and the cold-rolled SAF 2304 lean duplex steel was studied in acidified glycerin medium, collected directly from a biodiesel plant.

*e-mail: fernanda.menezes@ifmg.edu.br

Anodic potentiodynamic polarization procedure was used to evaluate the localized corrosion of steels at 337 K, a service temperature of the biodiesel plant. Cyclic potentiodynamic polarization technique was used with the objective to study the temperature influence on the materials' pitting corrosion and the repassivation behavior, at room temperature. Chronoamperometry was performed to analyze the protective characteristic of the passive layer by applying 0.1 V and 0.2 V (Ag/AgCl) potentials, with a duration of 2000 s at room temperature. Mott–Schottky analysis provided information about the passive films' dielectric properties at room temperature. Scanning electron microscopy (SEM) analysis and energy dispersive spectroscopy (EDS) were employed to characterize the corroded surfaces^{11,22,32-35}.

2. Experimental Procedure

2.1. Materials

The AISI 317L austenitic stainless steel and the cold-rolled SAF 2304 lean duplex stainless-steel chemical composition is shown in Table 1. Steels samples were provided by Aperam South America, Brazil. The samples were cut in 10 mm x 10 mm x 4 mm dimensions and mounted in epoxy resin. After that, the samples were polished using SiC paper of decreasing grit size: 100, 220, 400, and 600 mesh. The electric contact between the sample and the potentiostat was made by means of a welded copper wire. All edges were coated with insulating resin to avoid crevice occurrence during the experiments. The testing surfaces were washed with alcohol and dried.

2.2. Electrochemical measurements

The potentiodynamic polarization measurements were carried out according to the ASTM G-61 Standard³⁶. All the electrochemical experiments were performed in chloride-containing acidified glycerin solutions with 49.5 wt.% glycerin, 29 wt.% methanol, 17 wt.% water, 3 wt.% NaCl, and 1.5 wt.% organic materials, obtained from Petrobras Biocombustíveis. The anodic polarization test was performed at 337 K and the cyclic potentiodynamic polarization was done at room temperature. The temperature of 337 K was the service temperature from biodiesel production. The glycerin composition is shown in Table 2. An electrochemical system

with three electrodes was used: platinum as the counter electrode, Ag/AgCl as the reference electrode and the AISI 317L and SAF 2304 lean duplex stainless-steel samples as working electrodes.

The anodic polarization experiments were performed using IviumStat potentiostat and the data was obtained with IviumSoft software. Cyclic polarization, chronoamperometry and Mott–Schottky analysis were performed by using the PGSTAT100N system (Metrohm Autolab) and the NOVA 2.1 software. Before starting the anodic polarization test, the working electrode was immersed in the test solution for 3300 s and the open circuit potential (OCP) was measured. After the OCP achieved the equilibrium, the working electrode potential was scanned in the anodic direction from 50 mV below the OCP until 500 mV, at 0.167 mV/s scan rate. For the cyclic polarization procedure, the scan was reversed in the cathodic direction after reaching the potential of 700 mV. Each test was repeated at least three times to ensure reproducibility.

Chronoamperometry was carried out setting the potential of 0.1 V Ag/AgCl and 0.2 V Ag/AgCl for 2000 s.

Mott–Schottky analysis was carried out at a frequency of 1 kHz using a 10 mV ac signal and a step potential of 50 mV, in the cathodic direction from the initial potential of $-1.0 V_{Ag/AgCl}$ to the final potential of $1.0 V_{Ag/AgCl}$.

2.3. Surface characterization

The corroded surfaces were characterized by scanning electron microscopy (SEM) analysis, using the FEG - Quanta 200 FEI scanning electro-microscope equipped with an energy dispersive spectrometer (EDS) with a voltage of 30 kV and a working distance of 10 mm.

3. Result and Discussion

3.1. Electrochemical study

Figure 1 shows the anodic polarization curves for AISI 317L and SAF 2304 stainless steels (SS) in chloride-containing acidified glycerin solution, at 337 K. The data obtained from Figure 1 are shown in Table 3.

Both steel curves showed a typical active-passive-transpassive behavior in medium containing chloride with active dissolution, with passivation and the breakdown potentials³⁷.

Table 1. Chemical composition of AISI 317L and SAF 2304 (wt%) and Pitting Resistance Equivalent Number (PREN) values (Source: Aperam South America, Brazil).

Steel Type	UNS	C	Mn	Si	Cr	Ni	Mo	N	PRE
AISI 317L	S31700	0.03	2.00	0.75	19.00	13.00	3.50	0.06	31.51
SAF 2304	S32304	0.011	1.450	0.201	22.870	4.202	0.275	0.1193	25.69

Table 2. Glycerin characteristics (Source: Petrobras Biocombustíveis, Brazil).

Characteristics	Method	Result	Unit
pH	BIO 1012	6.17	-
Conductivity	STD 2510	4.90	mS/cm
Moisture	E203	14.94	%m/m
Acidity	CA 5A-40	0.1	%m/m

The pitting corrosion occurrence is indicated in the graph by a abrupt increase of the passivation current for a small variation of potential. The breakdown potential (E_{pit}) was given by the intersection between the tangents of the passive region and the transpassive region³⁸.

Pitting resistance equivalent number (PREN) is used to evaluate qualitatively steel's pitting corrosion resistance. This factor is correlated with the Cr, Mo and N chemical contents through the equation: $PRE = \%Cr + 3.3\%Mo + 16\%N^{11,30}$. According to PREN values presented in Table 1, AISI 317 has higher PREN than SAF 2304, indicating a higher corrosion resistance of AISI 317 than the SAF 2304. However, according to Mesquita et al.³⁹, PREN value does not consider the effects of the microstructure, surface condition, temperature, number of secondary inclusions, which influence the steel's corrosion behavior. Moreover, in duplex stainless steels, the chemical elements are not homogeneously distributed between the two phases. The Cr and Mo are preferably distributed in the ferrite phase and N and Ni elements are dispersed in the austenitic phase³⁴.

In Table 3, the E_{pit} value of SAF 2304 (322 ± 50 mV) was higher compared to AISI 317L (196 ± 55 mV), indicating a better corrosion behavior of the SAF 2304 due to the higher passive region. On the other hand, the I_{corr} value of SAF 2304 ($0.14 \pm 0.15 \mu A/cm^2$) was higher than AISI 317L ($0.023 \pm 0.008 \mu A/cm^2$). The high content of noble elements, such as nickel and molybdenum, in the AISI 317L SS contribute to the highest value of its E_{corr} and the lowest value of I_{pass} than SAF 2304. However, the chloride ions break through the AISI 317L SS passive layer more easily than they do through the layer of SAF 2304, since the E_{pit} value of SAF 2304 was higher compared to AISI 317L.

Table 3. Corrosion potential, corrosion current density, passivation potential, passive current density, and pitting potential average results of AISI 317L and SAF 2304 SS, in chloride-containing acidified glycerin solution at 337 K.

	AISI 317L	SAF 2304
E_{corr} (mV)	-34 ± 7	-67 ± 8
I_{corr} ($\mu A/cm^2$)	0.023 ± 0.008	0.14 ± 0.15
E_{pass} (mV)	-5.0 ± 2.4	-17 ± 3
I_{pass} ($\mu A/cm^2$)	0.22 ± 0.07	0.4 ± 0.03
E_{pit} (mV)	196 ± 55	322 ± 50

Table 4. Corrosion potential, corrosion current density, passivation potential, passivation current density, and pitting potential average results of AISI 317L SS and SAF 2304 SS in chloride-containing acidified glycerin solution at room temperature.

	AISI 317L	SAF 2304
E_{corr} (mV)	-44 ± 7	-230 ± 110
I_{corr} ($\mu A/cm^2$)	0.0027 ± 0.0010	0.17 ± 0.12
I_{pass} ($\mu A/cm^2$)	0.050 ± 0.027	6 ± 4
E_{pit} (mV)	330 ± 67	500 ± 33
E_{prot} (mV)	-	-26 ± 9

Cyclic potentiodynamic polarization testing was performed for AISI 317L and SAF 2304 SS in chloride-containing acidified glycerin solution, at room temperature, as shown in Figure 2. The data obtained from Figure 2 is shown in Table 4.

From the cyclic polarization tests, at room temperature, the E_{pit} value of SAF 2304 (500 ± 33 mV) was higher than AISI 317L (330 ± 67 mV). I_{pass} of SAF 2304 ($6 \pm 4 \mu A/cm^2$) was higher than the I_{pass} of the AISI 317L ($0.050 \pm 0.027 \mu A/cm^2$) as well. In Figure 2, notice that AISI 317L did not repassivate at the reverse scan and showed a positive hysteresis. The SAF 2304 also showed a positive hysteresis but repassivated in the reverse scan with a protection potential at -26 ± 9 mV.

Comparing Figures 1 and 2, it can be noted that as temperature decreased, there was an increase in the pitting potential of both steels, as was expected by the literature^{11,40}. Considering the breakdown potential, the SAF 2304 is more corrosion resistant than AISI 317L in both temperatures, 337 K and at room temperature. However, the I_{corr} and I_{pass} remained lower for AISI 317L compared with SAF 2304.

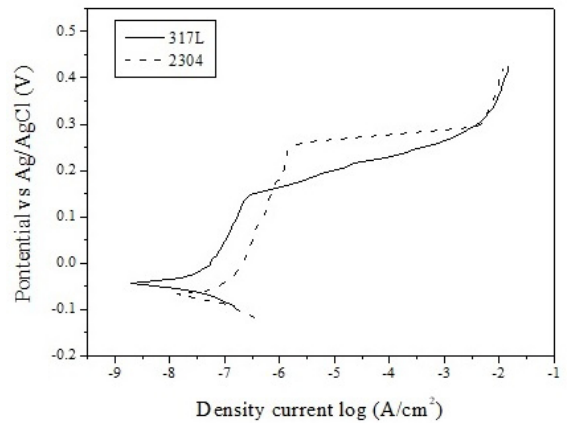


Figure 1. Anodic polarization curves of the AISI 317L and SAF 2304 SS in chloride-containing acidified glycerin solution at 337 K.

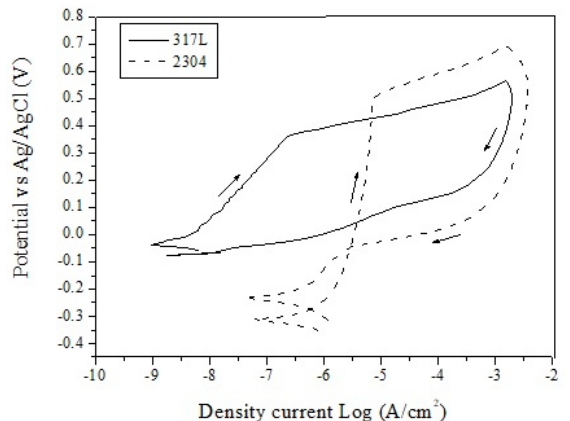


Figure 2. Cyclic polarization curves of AISI 317L and SAF 2304 SS in chloride-containing acidified glycerin solution at room temperature.

Considering that acidified glycerin is not a very aggressive medium to these steels (pH 6), the critical parameter in localized corrosion can be considered as the passive film properties in presence of chloride, evaluated by chronoamperometry and Mott–Schottky analysis⁴¹.

3.1.1. Chronoamperometry

For the Chronoamperometry test, a constant potential of 0.1 and 0.2 V (Ag/AgCl) was applied for 2000 s, as shown in Figures 3 and 4. These potential values were chosen based on the AISI 317L and the SAF 2304 passivation regions. With this fact, the AISI 317L and SAF 2304 passive layer stability was evaluated in chloride-containing acidified glycerin solution at room temperature.

It can be seen in Figure 3, for SAF 2304 and AISI 317L, that under 0.1 V, the current density was stable during the time analyzed. It also remained around the order of 10^{-7} A/cm² for both steels. The initial positive current peak (at zero time) can be due to the preexisting metal oxide dissolution on the surface⁴².

In Figure 4, under 0.2V the current density of SAF 2304 was not stable. It varied around 10^{-4} A/cm². On the other hand, the current density of AISI 317L was stable. It was around 10^{-6} A/cm². It can be concluded that the AISI 317L passive layer at 0.2 V (Ag/AgCl) was more protective than the passive layer of the SAF 2304. The chronoamperometry results corroborate with the polarization curve, because in Figures 1 and 2 the AISI 317L presented lower I_{pass} than the SAF 2304.

3.1.2. Mott–Schottky

The Mott-Schottky analysis of the passive film semiconducting characteristic formed on stainless steels can be used to support the study about corrosion resistance^{35,37,43,44}. However, the electronic properties of stainless steel's passive layers may be difficult to measure due the bilayer film's structure⁴⁴. The passive film on stainless steel is composed of two distinct layers. For most authors, the inner layer is rich in chromium oxide, Cr₂O₃, and the outer layer is a mixture of iron oxide, Fe₂O₃, and iron hydroxides^{34,35,45,46}.

Based on the point defect model (PDM), the point defects in the passive film are cation vacancies, oxygen vacancies, and cation interstitials. Cation vacancies are electron acceptors, and oxides with cation vacancies are considered a p-type barrier layer. Oxygen vacancies and metal ion interstitials are electron donors, resulting in n-type semiconductors. These passive films' semiconducting behavior depends on the relative number of defects within the film^{43,47,48}.

The Mott-Schottky analysis is based on the measured capacitance of the n-type and p-type semiconductor as a function of the applied potential, according to the Mott–Schottky equation described as^{37,41,46–48}:

$$\frac{1}{C^2} = \pm \frac{2}{Ne\epsilon\epsilon_0} \left(E - E_{fb} - \frac{kT}{e} \right) \quad (1)$$

where e is the electron charge (1.6029×10^{-19} C); N is the donor density for n-type semiconductor or the acceptor density for p-type semiconductor; ϵ is the semiconductor relative dielectric constant (for stainless steel, this value is $15.6^{43,47,48}$); ϵ_0 is the vacuum permittivity, $8.8542 \cdot 10^{-14}$ F/cm;

k is the Boltzmann's constant ($1.38 \cdot 10^{-23}$ J/K); T is the absolute temperature; E is the electrode potential and E_{fb} is the flat band potential.

From Equation 1, donor or acceptor density can be determined from the experimental C^{-2} vs E plots slope (m), as shown in Equation 2:

$$N = \frac{2}{me\epsilon\epsilon_0} \quad (2)$$

For a p-type semiconductor, the “ C^{-2} vs. E ” graphic has a negative slope, which is inversely proportional to the acceptor concentration. For a n-type semiconductor, “ C^{-2} vs. E ” graphic has a positive slope, inversely proportional to the donor concentration in the film. E_{fb} can be calculated by extrapolation, where $C^{-2} = 0^{33,37,47}$.

In this study, the Mott–Schottky analysis was performed to evaluate the passivation layer electrical properties of the AISI 317L and SAF 2304 in chloride-containing acidified glycerin, at room temperature. The results are shown in Figure 5 and Table 5.

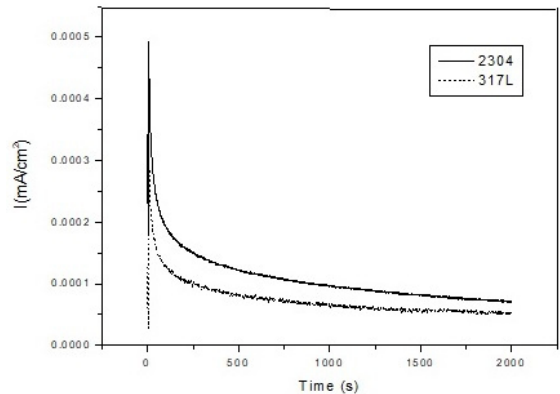


Figure 3. Chronoamperometry curves obtained for the AISI 317L and SAF 2304 in chloride-containing acidified glycerin solution at room temperature, applying 0.1V Ag/AgCl potential.

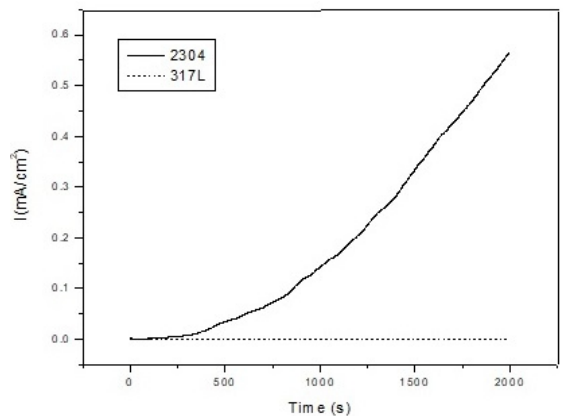


Figure 4. Chronoamperometry curves obtained for the AISI 317L and SAF 2304 in acidified glycerin solution containing chloride at room temperature, applying 0.2V Ag/AgCl potential.

In Figure 5, for AISI 317L and SAF 2304 samples, Mott-Schottky analysis revealed positive and negative slopes. These two regions can be related with the bilayer characteristics of the passive layer. The peak shape in Mott-Schottky plots indicate an inversion from p-type to n-type semiconductor, in which the two oxides are in the flat-band conditions⁴⁹. From cyclic polarization data, the passivation region (anodic domain) of AISI 317L was above -44mV and for SAF 2304 it was above -230mV. In this potential range in Mott-Schottky graph, Figure 5, it is possible to notice that the passive layer has a semiconducting behavior of n-type (cation vacancies). The literature affirms that the p-type semiconductor is related to the presence of chromium oxides and the n-type semiconductor behavior is from iron oxides^{49,50}.

In the n-type region, more than one slope can be found for AISI 317L and SAF 2304 (N_{D1} , N_{D2}). It can be explained by the non-uniform donor distribution within the film^{49,51}.

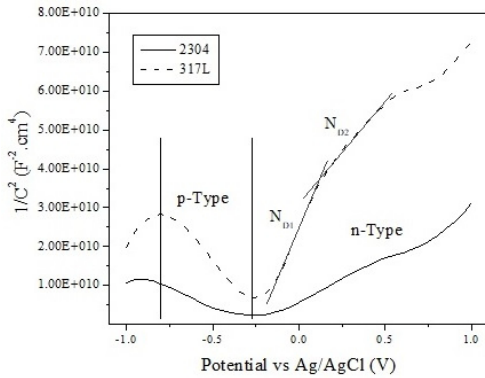


Figure 5. Mott-Schottky plots for the passive film formed on the AISI 317L and SAF 2304 SS, in chloride-containing acidified glycerin solution at room temperature.

According to Equation 2, the decrease of the slope is related with the increase in the donor density, which agrees with the increase of the current density due to corrosion reactions found in cyclic polarization results.

The acceptors and donor density, shown in Table 5, were calculated using Equation 2. N_d is the sum of all donors' levels. The orders of magnitude were around $10^{20} - 10^{21} \text{ cm}^{-3}$ and were comparable to the literature^{17,49,52}. The donor density was higher than the acceptor density in the passive film of both steels, which can be concluded again that the passive layer predominant properties were of n-type semiconductor. The higher donor density of SAF2304 compared to AISI 317L indicates a more active passive layer, however the SAF 2304 steel showed the highest E_{pit} .

3.2. Surface study

The SS samples surfaces, before and after the anodic potentiodynamic polarization and cyclic potentiodynamic polarization, were analyzed using scanning electron microscopy (SEM) analysis, as shown in Figure 6.

Figure 6 shows the microstructure difference between the analyzed steels. For the AISI 317L steel, Figure 6a shows only one surface phase, the austenite. Nevertheless, for the SAF 2304, in (Figure 6d), it is possible to visualize two distinct phases, a darker phase, ferrite (α), and a lighter phase, austenite (γ)^{18,19}. After electrochemical tests of AISI 317L SS surfaces, in Figures 6b and 6c, a localized corrosion occurred due to the presence of chlorides in glycerin.

Table 5. Acceptor density (N_a) and donor density (N_d) calculated from Mott-Schottky plots slope for the AISI 317L and SAF 2304, in chloride-containing acidified glycerin solution at room temperature.

Steel Type	$N_a (\text{cm}^{-3}) \cdot 10^{32}$	$N_d (\text{cm}^{-3}) \cdot 10^{32}$
AISI 317L	1.7	10
SAF 2304	5	13

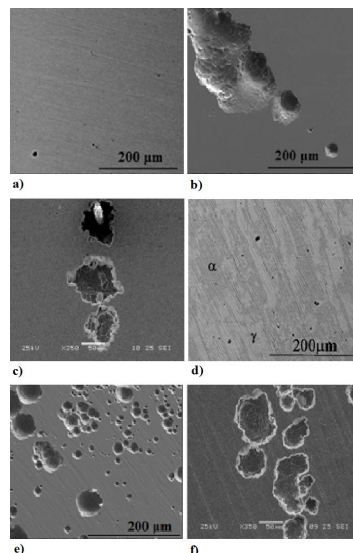


Figure 6. SEM micrographs for AISI 317L, before electrochemical test (a), after anodic polarization (b) and after cyclic polarization (c) and for SAF 2304, before electrochemical test (d), after anodic polarization (d) and after cyclic polarization (f).

Likewise, for SAF 2304 SS, Figures 6e and 6f, corrosion pits were observed on the steel surface. Moreover, comparing the pitting corrosion on AISI 317L, Figures 6b and 6c, and SAF 2304, Figures 6e and 6f, it is possible to notice a higher concentration of cavities. It agrees with anodic polarization, cyclic polarization, chronoamperometry, and Mott-Schottky results, where it could be concluded that the SAF 2304 had a less protective passivation layer than that of the AISI 317L, although the E_{pit} value of SAF 2304 was higher compared to AISI 317L.

4. Conclusion

This present work aimed to compare the corrosion resistance of SAF 2304 and AISI 317L SS in chloride-containing acidified glycerin solution using electrochemical and scanning electron microscopy techniques. The following conclusions could be driven:

- The increase in the temperature decreased the pitting potential of the AISI 317L and SAF 2304 in acidified glycerin. The increase in the temperature accelerates the conversion of pits from a metastable condition to a stable situation on the test medium.
- The SAF 2304 showed a higher pitting corrosion resistance than the AISI 317L, since it showed a higher breakdown potential than the AISI 317L, at room temperature and 337 K, in acidified glycerin from the biodiesel industry.
- The AISI 317L showed a more protective passive layer than SAF 2304, with a lower passive current density than the SAF 2304 steel at room temperature and at 337 K. At 0.1 V (Ag/AgCl) both steels had a constant passive current but at 0.2 V (Ag/AgCl), the SAF 2304 SS passive current density continuously increased with time in the acidified glycerin. The donor density of SAF 2304 was higher than AISI 317L as well.
- The AISI 317L showed a positive hysteresis and did not repassivate in the reverse scan in the acidified glycerin. The SAF 2304 showed a repassivation with a protection potential of -26 mV (Ag/AgCl).

5. References

1. Abbaszaadeh A, Ghobadian B, Omidkhan MR, Najafi G. Current biodiesel production technologies: a comparative review. *Energy Convers Manage*. 2012;63:138-48.
2. Fazal MA, Haseeb ASMA, Masjuki HH. Effect of different corrosion inhibitors on the corrosion of cast iron in palm biodiesel. *Fuel Process Technol*. 2011;92(11):2154-9.
3. Rajak U, Verma TM. *Spirulina* microalgae biodiesel: a novel renewable alternative energy source for compression ignition engine. *J Clean Prod*. 2018;201:343-57.
4. Coronado CR, Carvalho JA Jr, Silveira JL. Biodiesel CO₂ emissions: a comparison with the main fuels in the Brazilian market. *Fuel Process Technol*. 2009;90(2):204-11.
5. Thangaraja B, Solomon PR. Biodiesel production by the electrocatalytic process: a review. *Clean Energy*. 2001;5:9-31.
6. Hu XG, Zhou LL, Wang QJ, Xu YF, Zhu XF. On corrosion behaviour of metal in biomass. *Corros Eng Sci Technol*. 2011;46(4):400-5.
7. Pasqualino JC, Montané D, Salvadó J. Synergic effects of biodiesel in the biodegradability of fossil-derived fuels. *Biomass Bioenergy*. 2006;30(10):874-9.
8. Torres CEAS, Santos TE, Lins VFC. Corrosion failures of austenitic and duplex stainless steels in a biodiesel plant. *Materia*. 2020;25(2):e12620.
9. Adeli M, Golozar MA, Raeissi K. Pitting corrosion of SAF2205 duplex stainless steel in acetic acid containing bromide and chloride. *Chem Eng Commun*. 2010;197(11):1404-16.
10. Jafarian M, Gopal F, Danaee I, Biabani R, Mahjani MG. Electrochemical studies of the pitting corrosion of tin in citric acid solution containing Cl⁻. *Electrochim Acta*. 2008;53(13):4528-36.
11. Huang T, Tsai W-T, Pan S-J, Chang K-C. Pitting corrosion behaviour of 2101 duplex stainless steel in chloride solutions. *Corros Eng Sci Technol*. 2018;53(Suppl 1):9-15.
12. Wang W, Jenkins PE, Ren Z. Electrochemical corrosion of carbon steel exposed to biodiesel/simulated seawater mixture. *Corros Sci*. 2012;57:215-9.
13. Alves SM, Dutra-pereira FK, Bicudo TC. Influence of stainless steel corrosion on biodiesel oxidative stability during. *Fuel*. 2019;249:73-9.
14. Kugelmeier CL, Monteiro MR, da Silva R, Kuri SE, Sordi VL, Della Rovere CA. Corrosion behavior of carbon steel, stainless steel, aluminum and copper upon exposure to biodiesel blended with petrodiesel. *Energy*. 2021;226:120344.
15. Eghbali F, Moayed MH, Davoodi A, Ebrahimi N. Critical pitting temperature (CPT) assessment of 2205 duplex stainless steel in 0.1M NaCl at various molybdate concentrations. *Corros Sci*. 2011;53(1):513-22.
16. Torres CEAS, Costa CGF, Pereira AP, Castro MMR, Lins VFC. Corrosion failure analysis in a biodiesel plant using electrical resistance probes. *Eng Fail Anal*. 2016;66:365-72.
17. Sicupira DC, Cardoso R Jr, Bracarense AQ, Frankel GS, Lins VFC. Cyclic polarization study of thick welded Joints of lean duplex stainless steel for application in biodiesel Industry. *Mater Res*. 2016;20(1):161-7.
18. Sicupira DC, Cardoso R Jr, Bracarense AQ, Frankel GS, Lins VFC. Electrochemical study of passive films formed on welded lean duplex stainless steel. *Mater Corros*. 2017;68(6):604-12.
19. Sicupira DC, Frankel GS, Lins VFC. Pitting corrosion of welds in UNS S32304 lean duplex stainless steel. *Mater Corros*. 2016;67(5):440-8.
20. Ma L, Pascalidou E-M, Wiame F, Zanna S, Maurice V, Marcus P. Passivation mechanisms and pre-oxidation effects on model surfaces of FeCrNi austenitic stainless steel. *Corros Sci*. 2020;167:108483.
21. Ferreira EA, Della Noce R, Fugivaram CS, Benedetti AV. Influence of ethanol, acidity and chloride concentration on the corrosion resistance of AISI 316L stainless steel. *J Braz Chem Soc*. 2013;24(3):397-405.
22. Tranchida G, Clesi M, Di Franco F, Di Quarto F, Santamaria M. Electronic properties and corrosion resistance of passive films on austenitic and duplex stainless steels. *Electrochim Acta*. 2018;273:412-23.
23. Loto CA, Popoola API, Fayomi OS, Loto RT. Corrosion polarization behaviour of type 316 stainless steel in strong acids and acid chlorides. *Int J Electrochem Sci*. 2012;7(4):3787-97. [http://dx.doi.org/10.1016/S1452-3981\(23\)13997-6](http://dx.doi.org/10.1016/S1452-3981(23)13997-6).
24. Ait Albrimi Y, Ait Addi A, Douch J, Souto RM, Hamdani M. Inhibition of the pitting corrosion of 304 stainless steel in 0.5M hydrochloric acid solution by heptamolybdate ions. *Corros Sci*. 2015;90:522-8. <http://dx.doi.org/10.1016/j.corsci.2014.10.023>.
25. Ostovan F, Shafiei E, Toozandehjani M, Mohamed IF, Soltani M. On the role of molybdenum on the microstructural, mechanical and corrosion properties of the GTAW AISI 316 stainless steel welds. *J Mater Res Technol*. 2021;13:2115-25.
26. Mottu N, Vayer M, Dudognon J, Erre R. Structure and composition effects on pitting corrosion resistance of austenitic stainless steel after molybdenum ion implantation. *Surf Coat Tech*. 2005;200(7):2131-6.
27. Miranda-Pérez AF, Rodríguez-Vargas B, Calliari I, Pezzato L. Corrosion resistance of GMAW duplex stainless steels welds. *Materials*. 2023;16(5):1847.

28. Gennari C, Pezzato L, Tarabotti G, Zamboni A, Di Schino A, Calliari I. Influence of electropulsing treatments on mechanical properties of UNS S32750 duplex stainless steel. *Materials*. 2020;13(7):1613.
29. Silva R, Kugelmeier CL, Vacchi GS, Martins CB, Dainezi I, Afonso CRM, et al. A comprehensive study of the pitting corrosion mechanism of lean duplex stainless steel grade 2404 aged at 475 °C. *Corros Sci*. 2021;191:109738.
30. Cvijović Z, Radenković G. Microstructure and pitting corrosion resistance of annealed duplex stainless steel. *Corros Sci*. 2006;48(12):3887-906.
31. Tavares SSM, Pardal JM, Silva MR, Oliveira CAS. Martensitic transformation induced by cold deformation of lean duplex stainless steel UNS S32304. *Mater Res*. 2013;17(2):381-5.
32. Ferreira DGO, Torres CEAS, Lins VFC, Park SW. Computational fluid dynamics investigation for austenitic AISI 904L stainless steel corrosion in a biodiesel stream pipping. *Material and Corrosion*. 2018;69(2):266-79.
33. Izquierdo J, Martín-Ruiz L, Fernández-Pérez BM, Rodríguez-Raposo R, Santana JJ, Souto RM. Scanning microelectrochemical characterization of the effect of polarization on the localized corrosion of 304 stainless steel in chloride solution. *J Electroanal Chem*. 2014;728:148-57.
34. Wang Z, Seyeux A, Zanna S, Maurice V, Marcus P. Chloride-induced alterations of the passive film on 316L stainless steel and blocking effect of pre-passivation. *Electrochim Acta*. 2020;329:135159.
35. Hakiki NE. Comparative study of structural and semiconducting properties of passive films and thermally grown oxides on AISI 304 stainless steel. *Corros Sci*. 2011;53(9):2688-99.
36. ASTM: American Society for Testing and Materials. ASTM G-61: standard test method for conducting cyclic potentiodynamic polarization measurements for localized corrosion susceptibility of iron, nickel or cobalt based alloys. West Conshohocken: ASTM; 2009.
37. Freire L, Carmezim MJ, Ferreira MGS, Montemor MF. The electrochemical behaviour of stainless steel AISI 304 in alkaline solutions with different pH in the presence of chlorides. *Electrochim Acta*. 2011;56(14):5280-9.
38. Alonso-Falleiros N, Wolyneć S. Correlation between corrosion potential and pitting potential for AISI 304L austenitic stainless steel in 3.5% NaCl aqueous solution. *Mater Res*. 2002;5(1):77-84.
39. Mesquita TJ, Chauveau E, Mantel M, Kinsman N, Roche V, Nogueira RP. Lean duplex stainless steels: the role of molybdenum in pitting corrosion of concrete reinforcement studied with industrial and laboratory castings. *Mater Chem Phys*. 2012;132(2-3):967-72.
40. Li DG, Wang JD, Chen DR, Liang P. Influences of pH value, temperature, chloride ions and sulfide ions on the corrosion behaviors of 316L stainless steel in the simulated cathodic environment of proton exchange membrane fuel cell. *J Power Sources*. 2014;272:448-56.
41. Frankel GS, Li T, Scully JR. Localized corrosion: passive film breakdown vs pit growth stability. *J Electrochem Soc*. 2017;164(4):C180-1.
42. Abbott AP, Capper G, McKenzie KJ, Ryder KS. Voltammetric and impedance studies of the electropolishing of type 316 stainless steel in a choline chloride based ionic liquid. *Electrochim Acta*. 2006;51(21):4420-5.
43. Fernández-Domene RM, Blasco-Tamarit E, García-García DM, García-Antón J. Effect of alloying elements on the electronic properties of thin passive films formed on carbon steel, ferritic and austenitic stainless steels in a highly concentrated LiBr solution. *Thin Solid Films*. 2014;558:252-8.
44. Tranchida G, Clesi M, Di Franco F, Di Quarto F, Santamaria M. Electronic properties and corrosion resistance of passive films on austenitic and duplex stainless steels. *Electrochim Acta*. 2018;273:412-23.
45. Fattah-alhosseini A, Vafaiean S. Comparison of electrochemical behavior between coarse-grained and fine-grained AISI 430 ferritic stainless steel by Mott-Schottky analysis and EIS measurements. *J Alloys Compd*. 2015;639:301-7.
46. Luo H, Dong CF, Cheng XQ, Xiao K, Li XG. Electrochemical behavior of 2205 duplex stainless steel in NaCl solution with different chromate contents. *J Mater Eng Perform*. 2012;21(7):1283-91.
47. Fattah-alhosseini A, Golozar MA, Saatchi A, Raeissi K. Effect of solution concentration on semiconducting properties of passive films formed on austenitic stainless steels. *Corros Sci*. 2010;52(1):205-9.
48. Ferreira DGO, Torres CEAS, Lins VFC, Park SW. Computational fluid dynamics investigation for austenitic AISI 904L stainless steel corrosion in a biodiesel stream pipping. *Mater Corros*. 2018;69(2):266-79.
49. Metikoš-Huković M, Babić R, Grubač Z, Petrović Ž, Lajčič N. High corrosion resistance of austenitic stainless steel alloyed with nitrogen in an acid solution. *Corros Sci*. 2011;53(6):2176-83.
50. Luo H, Dong CF, Xiao K, Li XG. Characterization of passive film on 2205 duplex stainless steel in sodium thiosulphate solution. *Appl Surf Sci*. 2011;258(1):631-9.
51. Guo HX, Lu BT, Luo JL. Study on passivation and erosion-enhanced corrosion resistance by Mott-Schottky analysis. *Electrochim Acta*. 2006;52(3):1108-16.
52. Feng Z, Cheng X, Dong C, Xu L, Li X. Passivity of 316L stainless steel in borate buffer solution studied by Mott-Schottky analysis, atomic absorption spectrometry and X-ray photoelectron spectroscopy. *Corros Sci*. 2010;52(11):3646-53.